# Inhibition of Transport of a Bose-Einstein Condensate in a Random Potential

Jocelyn A. Retter, Andrès F. Varòn, David Clément, Mathilde Hugbart, Philippe Bouyer, Laurent Sanchez-Palencia, Dmitry Gangardt, Gora V. Shlyapnikov, Alain Aspect

# INHIBITION OF TRANSPORT OF A BOSE-EINSTEIN CONDENSATE IN A RANDOM POTENTIAL

J. A. RETTER[1], A. F. VARÓN[1], D. CLÉMENT[1], M. HUGBART[1], P. BOUYER[1], L. SANCHEZ-PALENCIA[1], D. GANGARDT[2], G. V. SHLYAPNIKOV[2,3], AND A. ASPECT[1]

[1] *Laboratoire Charles Fabry de l'Institut d'Optique, Université Paris-Sud XI, 91403 Orsay cedex, France.*
[2] *Laboratoire de Physique Théorique et Modèles Statistiques, Université Paris-Sud XI, 91405 Orsay cedex, France.*
[3] *Van der Waals-Zeeman Institute, University of Amsterdam, Valckenierstraat 65/67, 1018 XE Amsterdam, The Netherlands.*

We observe the suppression of the 1D transport of an interacting elongated Bose-Einstein condensate in a random potential with a standard deviation small compared to the typical energy per atom, dominated by the interaction energy. Numerical solutions of the Gross-Pitaevskii equation reproduce well our observations. We propose a scenario for disorder-induced trapping of the condensate in agreement with our observations[1].

## 1. Introduction

Coherent transport of waves in disordered systems is a topic of primary importance in condensed-matter physics, for example in the description of normal metallic conduction, superconductivity and superfluid flow, and has relevance also to optics and acoustics[2]. The presence of disorder can lead to intriguing and non-intuitive phenomena such as Anderson localization[3], percolation dynamics[4], and disorder-driven quantum phase transitions to Bose-glass[5] or spin-glass[6] phases. The main difficulty in understanding quantum transport arises from the subtle interplay of scattering on the potential landscape, interferences and interparticle interactions. Due to a high degree of control and measurement possibilities, dilute atomic Bose-Einstein condensates in optical potentials have proved an ideal system in which to revisit traditional condensed matter problems, and recent theoretical works discuss disorder-induced phenomena in this context[7]. Apart from the (undesired) effect of a rough potential on trapped cold atoms on atom

chips[8], there have been few experiments on BEC in random potentials[9,10].

In this experiment[1], we study the axial expansion of an elongated BEC in a magnetic guide, in the presence of a disordered potential generated by laser speckle. We observe that a weak disordered potential inhibits both the expansion and the centre-of-mass (COM) motion of the condensate.

## 2. Laser Speckle — a disordered potential for atoms

Laser speckle[11] is the random intensity pattern produced when coherent laser light is scattered from a rough surface. Such patterns arise from interferences between wavefronts coming from different scattering sites. In the Fraunhofer limit, a speckle pattern does not depend on the details of the scattering surface, but follows a well-defined statistical distribution. The intensity distribution is exponential $P(I) = \exp(-I/\sigma_I)$ with the intensity standard deviation equal to the local mean intensity: $\sigma_I = \langle I(z) \rangle$. The typical distance $\Delta z$ between speckle 'grains' can be characterised by the half-width of the autocorrelation function. For a circular aperture, this is an Airy function, with the first zero located at $\Delta z = 1.22\lambda l/D$, where $\lambda$ is the laser wavelength, $l$ the distance from the scattering plate to the observation plane, and $D$ the aperture diameter at the scattering surface.

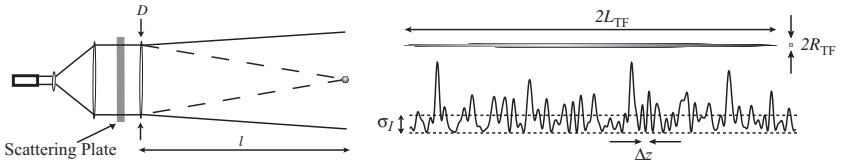


Figure 1. Left: Optical setup used to create the random speckle potential. The condensate is at the focal point of the lens system, with its long axis oriented perpendicular to the page. Right: Example of speckle intensity profile, with condensate to scale. The speckle potential is effectively 1D for the trapped condensate.

In our experiment, a blue-detuned laser beam is shone onto the atoms through a scattering plate, as shown in Fig. 1. The beam is derived from a tapered amplifier, injected by a free-running diode laser at $\lambda \sim 780\,\mathrm{nm}$ and fibre-coupled to the experiment. The out-coupled beam is expanded and then focused onto the condensate, the fibre out-coupler and lenses being mounted on a single small optical bench, aligned perpendicular to the long axis of the BEC. Inserting the scattering plate in the position shown projects an optical speckle potential onto the atoms, with an intensity dis-

tribution $I(\mathbf{r})$ which is simply the Fourier transform of the phase distribution at the scattering plate. The scattered beam has a total power of up to 150 mW and diverges to an rms radius of 1.83 mm at the condensate. The mean intensity (the gaussian envelope) of the beam can be assumed constant over the region where the atoms are trapped.

To calibrate the speckle pattern, the optical set-up is removed from the BEC apparatus and the intensity distribution observed on a CCD camera at the same distance $l$ as the atoms. Taking images with various beam apertures $D$, we verify the exponential intensity distribution $P(I)$, and compute the autocorrelation function to obtain the grain size $\Delta z$. Taking into account the modulation transfer function of the camera[12], we find that the measured grain size follows the prediction. For our setup, $l = 140(5)$ mm and $D = 25.4(1)$ mm, giving $\Delta z = 5.2(2)$ $\mu$m. In this experiment, we produce condensates with an aspect ratio of 100, typical Thomas-Fermi half-length $L_{\rm TF} = 150\,\mu$m and radius $R_{\rm TF} = 1.5\,\mu$m. The trapped BEC occupies about 45–50 minima along its length, but experiences an almost constant potential in the radial directions. (Along the axis of the laser beam, the typical length scale of the speckle grains is much longer, $\sim \Delta z^2/\lambda = 35\,\mu$m.) The speckle potential is therefore effectively one-dimensional (1D) for the atoms: $R_{\rm TF} < \Delta z \ll L_{\rm TF}$. This is important as systems in 1D potentials are known to be more sensitive to the effects of disorder[13].

We calibrate the speckle intensity $\langle I(z)\rangle$ as a function of the fibre-coupled laser power, from which the light-shift potential $V(z) \propto I(z)/\delta$ is determined[1]. The longitudinal positioning of the optical set-up at a distance $l$ from the atoms is controlled to within 5 mm, leading to an uncertainty of 3.5% on the speckle intensity. Since the light is blue-detuned from resonance ($|\delta| > 0.15$ nm), the potential is *repulsive* for the atoms. For the laser intensities used in this experiment, the standard deviation of the optical potential $\sigma_V = \langle V(z)\rangle$ is always smaller than the chemical potential $\mu$ of the condensate.

Other recent experiments have also generated disordered optical potentials for BEC: using red-detuned laser speckle[9] and by imaging randomly patterned structures onto an optical lattice[10].

## 3. Experimental Sequence

**Condensate preparation.** We generate an elongated (quasi-1D) BEC of $^{87}$Rb atoms in the $5S_{1/2}|F = 1, m_F = -1\rangle$ state, using an iron-core electromagnet Ioffe-Pritchard trap[14] with final trap frequencies of

$\omega_\perp = 2\pi \times 660(4)\,\mathrm{Hz}$ radially and $\omega_z = 2\pi \times 6.70(7)\,\mathrm{Hz}$ axially. We obtain condensates of typically $3.5 \times 10^5$ atoms and chemical potential $\mu/2\pi\hbar \sim 5\,\mathrm{kHz}$. In such an elongated trapping geometry, phase fluctuations can be important[15]. However, at our estimated temperature of 150 nK, the phase coherence length is of the order of the condensate length.

The laser speckle is turned on at the end of the rf evaporation ramp and we wait a further 200 ms in the presence of the rf field to ensure that the condensate is in equilibrium at the end of the sequence.

**Axial expansion.** We next open the magnetic trap in the axial (dipole) direction while keeping the transverse confinement and the random potential unchanged, thus converting the trap into a long, uniform, magnetic guide. The condensate expands along this guide, the axial expansion being driven by the repulsive interatomic interactions.

Due to hysteresis in the electromagnet and coupling between the dipole and quadrupole poles, remanent magnetizations can produce an axial trapping potential even when the dipole excitation current is reduced to zero. For this reason it is necessary to invert the current in the dipole excitation coils. To avoid spin-flip losses to non-trapped hyperfine states, the minimum magnetic field must not cross zero, thus setting a lower limit for the dipole current. By extrapolating the variation of the condensate dipole mode frequency with the current, we estimate the final axial trapping frequency to be less than $\omega_z \sim 2\pi \times 0.4\,\mathrm{Hz}$, which is compatible with the linear expansion observed (see Fig. 2). The trap opening is carried out over 30 ms, in order to minimize trap loss and heating. Numerical simulations of the 3D Gross-Pitaevskii (GP) equation confirm that this 'slow' relaxation of the axial confinement reduces only slightly (by $\sim 4\,\%$) the asymptotic expansion velocity of the BEC with respect to a 'sudden' trap opening.

**Imaging.** After an axial expansion time $\tau$, the magnetic fields and laser speckle are switched off and the condensate is imaged by absorption after a further 15 ms time-of-flight. From axial profiles of these images, the COM position and rms half-length $L$ of the atomic cloud are determined.

## 4. Inhibition of Transport

In Fig. 2a we plot the half-length $L$ and COM position of the condensate as a function of axial expansion time $\tau$. In the absence of the speckle potential, the condensate expands axially, reaching a linear expansion velocity of $2.47(3)\,\mathrm{mm\,s^{-1}}$, consistent with the numerical predictions of the GP equation. When a small speckle potential $\sigma_V = 0.2\gamma$ is applied, the expansion is

decelerated and the BEC eventually stops expanding. This effect becomes more pronounced at higher speckle potentials, as shown in Fig. 2b. The BEC also acquires a constant COM velocity of $5.1(2)\,\mathrm{mm\,s^{-1}}$ due to a magnetic 'kick' during the trap-opening. This motion too is decelerated and finally stopped in the presence of a weak speckle potential.

By displacing the speckle potential by small distances in the vertical (radial) direction, we can project a completely different realization of the speckle potential onto the atoms. Since the BEC in the magnetic trap already covers many peaks of the speckle potential, we find that the expansion dynamics are fairly insensitive to the exact random potential.

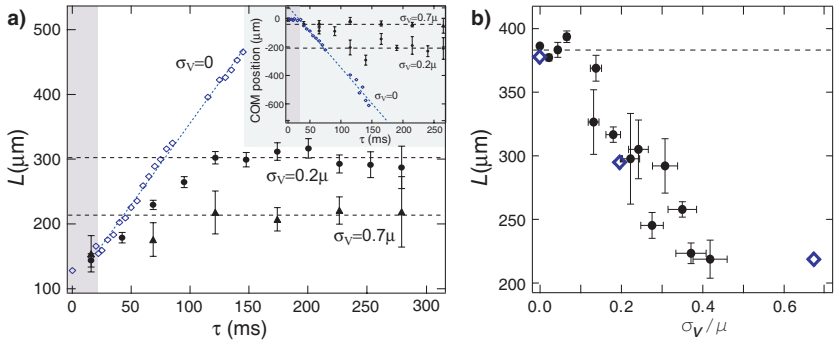


Figure 2. **a)** Rms half-length $L$ and COM position (inset) of the BEC as a function of axial expansion time $\tau$, for three different amplitudes of the disordered potential: $\sigma_V = 0,\ 0.2\mu,\ 0.7\mu$. The axial confinement is relaxed during the first 30 ms (grey band). **b)** Variation of rms half-length $L$ with speckle potential $\sigma_V$ for $\tau = 115\,\mathrm{ms}$. The three points $\diamondsuit$ correspond to the data shown in **a)**.

## 5. 'Disorder-induced trapping'

We are able to interpret the observed behaviour by studying the density profiles obtained by numerical integration of the GP equation. By assuming tight radial confinement, that is $\hbar\omega_\perp \gg \hbar\omega_z, \mu, k_\mathrm{B}T$, this equation is simplified to 1D. The static speckle potential is generated numerically, with $\Delta z = 0.049 L_\mathrm{TF}$. In Fig. 3 we see that this model reproduces well the trends observed experimentally, despite the approximation to 1D.

In the harmonic trap, the BEC is in the interaction-dominated, Thomas-Fermi regime: $n(z, t=0) = \max(0, \mu - 0.5 m\omega_z^2 z^2 - V(z))/g_{1D}$. Since the BEC healing length $\xi$ is much smaller than $\Delta z$, the density profile simply

follows the modulations of the speckle potential. These modulations are not sufficiently strong to fragment the BEC, as $\sigma_V < \mu$. After switching off the axial confinement, the BEC expands (for $\sigma_V = 0$) according to the scaling theory[16]. For times $\omega_z \tau \gtrsim 1$ the fastest atoms populate the wings of the BEC, where the density is lowest; conversely, at the centre of the BEC, the density and therefore the interaction energy remain relatively high, and the kinetic energy very low. In the presence of disorder we can therefore expect very different behaviour in each of these two regions.

Figure 3 shows a simulated density profile obtained for $\sigma_V = 0.2\mu$ and $\omega_z \tau = 10$, at which time the BEC has stopped expanding. Looking more closely at the central region $-L_{\rm TF}/2 < z < L_{\rm TF}/2$ (Fig. 3a) we find that the condensate density modulations have mainly the same length-scale as the speckle potential, and that these modulations are stationary. Since in this

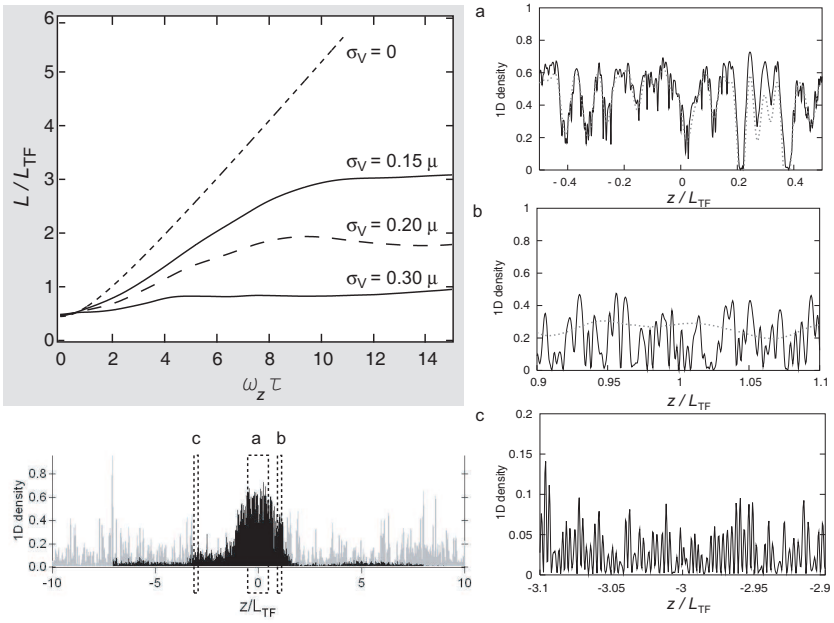


Figure 3. **Top** Time evolution of the rms size $L$ of the BEC in the random potential, for various speckle amplitudes $\sigma_V$, as obtained by numerical integration of the 1D GP equation. **Bottom** Simulated density profile (solid) at time $\omega_z \tau = 10$ during axial expansion, with $\sigma_V = 0.2\mu$ (grey line represents $V(z)/g_{1D}$). **Right** Zoom on density profile (solid) — note the different length scales. The approximation $n(z) = \max(0, \overline{\mu}(t) - V(z))/g_{1D}$ (dashed) reproduces the density only in the central region (a) (see text).

region the interaction energy remains dominant, we can suppose that the Thomas-Fermi approximation still holds. By defining an effective chemical potential $\overline{\mu}(t)$, which decreases with the density during expansion, we can write the density profile as: $n(z,t) = \max(0, \overline{\mu}(t) - V(z))/g_{1D}$. This is a good approximation close to $z = 0$ (see Fig. 3a), showing that the local density adiabatically adapts to the speckle potential as $\overline{\mu}(t)$ decreases. In this central region, the expansion stops when the condensate encounters two large peaks of the speckle potential with amplitudes larger than $\overline{\mu}(t)$, and the condensate then fragments.

In the low density regions, for example $-3.1L_{\rm TF} < z < -2.9L_{\rm TF}$ (Fig. 3c), the density profile is not stationary, and furthermore the length-scale of the density modulations is much smaller than $\Delta z$. By using Fourier analysis, we identify the characteristic length-scale as the healing length of the trapped condensate, $\xi = \hbar/\sqrt{2m\mu}$. This can be understood by conservation of energy, implying that the kinetic energy per atom is of the order of the typical energy per atom $\mu$, of the initial BEC. In this region, the atoms are therefore almost free particles, interacting with the disordered potential. The BEC wavefunction undergoes disorder-induced multiple transmissions and reflections and is ultimately blocked by a high peak $V(z) > \mu$ of the speckle potential. The continually evolving contributions of the low-density wings of the BEC are responsible for the fluctuations of $L$ observed in the simulation for $\sigma_V \gtrsim 0.2\mu$, even once the core of the wavefunction is localized. At intermediate distances (Fig. 3b), the Thomas-Fermi approximation is no longer valid, and the density profile exhibits time-dependent modulations with a length scale intermediate of $\xi$ and $\Delta z$.

To understand the role of the disordered potential in this trapping scenario, it is useful to compare this situation with that of a periodic potential, with a lattice spacing $\Delta z$ and depth $V_0 = 2\sigma_V$. Our model predicts similar behaviour in the central region, but differs in the low density wings, where the condensate would continue to expand due to tunnelling between the lattice sites. In the lattice, the condensate fragments when the central density reaches the value $n_0 \backsimeq V_0/g_{1D}$, independent of the lattice spacing. In the case of the disordered potential, this final density depends on the statistical distribution of the optical potential. We can calculate the probability of finding two speckle peaks of a given height within a given distance, which when combined with the condensate expansion dynamics leads to the following estimate for the final peak density: $n_0 \backsimeq 1.25(\sigma_V/g_{1D}) \ln(0.47L_{\rm TF}/\Delta z)$. This formula, dependent on both $\sigma_V$ and $\Delta z$, is in good agreement with our numerical findings and will be the subject of future experimental work[17].

## 6. Conclusion

We have investigated the transport properties of a BEC in a disordered potential, observing a cross-over from free expansion to absence of diffusion as the strength of the disorder increases. Our experimental findings are supported by numerical simulations and we have discussed a theoretical model which describes a scenario for disorder-induced trapping. In the future it would be interesting to further investigate this highly controllable system, for example by changing the correlation length of the disorder or using Bragg spectroscopy to probe the momentum spectrum of the BEC.

This work is supported by the CNRS, Ministère de la Recherche, DGA, EU (IST-2001-38863, MRTN-CT-2003-505032), ESF (BEC2000+), Marie Curie Fellowship (J.R.), IXSEA-OCEANO (M.H.) and INTAS (211-855).

## References

1. D. Clément *et al.*, to be published in Phys. Rev. Lett.; cond-mat/0506638.
2. E. Akkermans and G. Montambaux, *Physique Mésoscopique des Électrons et des Photons*, (EDP Science ed., Paris 2004).
3. P. W. Anderson, Phys. Rev. **109**, 5 (1958); Y. Nagaoka and H. Fukuyama (Eds.), *Anderson Localization*, Springer Series in Solid State Sciences No. 39, (Springer, Berlin, 1982); T. Ando and H. Fukuyama (Eds.), *Anderson Localization*, Springer Proceedings in Physics No. 28, (Springer, Berlin, 1988).
4. A. Aharony and D. Stauffer, *Introduction to Percolation Theory* (Taylor & Francis, London, 1994).
5. M. P. A. Fisher, P. B. Weichman, G. Grinstein, and D. S. Fisher, Phys. Rev. B **40**, 546 (1989).
6. M. Mézard, G. Parisi, and M. A. Virasoro, *Spin Glass and Beyond* (World Scientific, Singapore, 1987).
7. B. Damski *et al.*, Phys. Rev. Lett. **91**, 080403 (2003); R. Roth and K. Burnett, J. Opt. B **5**, S50 (2003); L. Sanchez-Palencia and L. Santos, cond-mat/0502529; A. Sanpera *et al.*, Phys. Rev. Lett. **93**, 040401 (2004).
8. see *e.g.* J. Estève *et al.*, Phys. Rev. A 043629 (2004) and references therein.
9. J. E. Lye *et al.*, cond-mat/0412167; C. Fort *et al.*, cond-mat/0507144.
10. T. Schulte *et al.*, cond-mat/0507453.
11. J. W. Goodman, in *Laser Speckle and Related Phenomena*, edited by J. C. Dainty (Springer-Verlag, Berlin, 1975).
12. M. Hugbart *et al.*, Eur. Phys. J. D **35**, 155 (2005); cond-mat/0501456.
13. D. J. Thouless, Phys. Rev. Lett. **39**, 1167 (1977).
14. V. Boyer *et al.*, Phys. Rev. A **62**, 021601 (2000).
15. D. S. Petrov, G. V. Shlyapnikov, and J. T. M. Walraven, Phys. Rev. Lett. **87**, 050404 (2001); S. Richard *et al.*, Phys. Rev. Lett. **91**, 010405 (2003).
16. Yu. Kagan, E. L. Surkov, and G. V. Shlyapnikov, Phys. Rev. A **54**, R1753 (1996); Y. Castin and R. Dum, Phys. Rev. Lett. **77**, 5315 (1996).
17. Further details of these properties will be described in a future publication.